Regional benthic δ^{18}O stacks for the "41-kyr world" - an Atlantic-Pacific divergence between 1.8-1.9 Ma

Yuxin Zhou[1], Lisiecki Lorraine[2], Taehee Lee[3], Geoffrey Gebbie[4], and Charles E Lawrence[3]

[1]University of California Santa Barbara
[2]University of California, Santa Barbara
[3]Brown University
[4]Woods Hole Oceanographic Institution

December 27, 2023

Abstract

Benthic δ^{18}O stacks are the benchmarks by which paleoceanographic data are stratigraphically aligned and compared. However, a recent study found that between 1.8-1.9 million years ago (Ma) several Ceara Rise records differed substantially from the widely used LR04 global stack. Here, we use new Bayesian stacking software to construct regional stacks and demonstrate a geographical divergence in benthic δ^{18}O features from 1.8-1.9 Ma. The pattern of isotopic stage features observed in the Ceara Rise is widespread throughout the Atlantic and differs notably from Pacific records. We propose that this regional difference in isotopic stages may be the result of relatively strong precession forcing and weaker obliquity forcing between 1.8-1.9 Ma. In accordance with the Antiphase Hypothesis, our results highlight a period of apparent sensitivity to regional precession forcing that is masked during most of the 41-kyr world due to the amplitude modulation of obliquity forcing.

Hosted file

982195_0_art_file_11688138_s5nbgz.docx available at https://authorea.com/users/103448/articles/693990-regional-benthic-%CE%B4180-stacks-for-the-41-kyr-world-an-atlantic-pacific-divergence-between-1-8-1-9-ma

Regional benthic $\delta^{18}O$ stacks for the "41-kyr world" - an Atlantic-Pacific divergence between 1.8-1.9 Ma

Yuxin Zhou[1], Lorraine E. Lisiecki[1], Taehee Lee[2], Geoffrey Gebbie[3], and Charles Lawrence[2]
[1]Department of Earth Science, University of California, Santa Barbara.
[2]Division of Applied Mathematics, Brown University.
[3]Physical Oceanography Department, Woods Hole Oceanographic Institution.
Corresponding author: Yuxin Zhou (yuxin_zhou@ucsb.edu)

Key points

- New Atlantic and Pacific benthic $\delta^{18}O$ stacks show different patterns between 1.8-1.9 Ma.
- The Atlantic-Pacific difference in this portion of the 41-kyr world may be caused by regional sensitivity to relatively strong precession.
- Regional benthic $\delta^{18}O$ stacks are preferable to global stacks for stratigraphic alignment.

Abstract

Benthic $\delta^{18}O$ stacks are the benchmarks by which paleoceanographic data are stratigraphically aligned and compared. However, a recent study found that between 1.8-1.9 million years ago (Ma) several Ceara Rise records differed substantially from the widely used LR04 global stack. Here, we use new Bayesian stacking software to construct regional stacks and demonstrate a geographical divergence in benthic $\delta^{18}O$ features from 1.8-1.9 Ma. The pattern of isotopic stage features observed in the Ceara Rise is widespread throughout the Atlantic and differs notably from Pacific records. We propose that this regional difference in isotopic stages may be the result of relatively strong precession forcing and weaker obliquity forcing between 1.8-1.9 Ma. In accordance with the Antiphase Hypothesis, our results highlight a period of apparent sensitivity to regional precession forcing that is masked during most of the 41-kyr world due to the amplitude modulation of obliquity forcing.

Plain language summary

To determine the age of deep-sea sediments, often the oxygen isotope ratios of microfossils are measured and compared to a previously compiled global benchmark. Recently, one of the most widely used oxygen isotope benchmarks has been challenged based on a comparison with several Atlantic records. In this study we assess several lines of evidence including utilizing newly available data and software. We confirm the challenge to the global oxygen isotope benchmark and find that it is more widespread than originally realized. Particularly, we find that oxygen isotope records display different patterns between the Atlantic and Pacific Oceans from 1.8-1.9 million years ago (Ma). We propose that this difference is the result of the opposing seasonal solar radiation anomalies received by the northern and southern hemispheres, which exhibited particularly large amplitudes during this time. Our study adds supporting evidence to a hypothesis that explains the dominant frequency of climatic cycles from 1.2-2.6 Ma.

Introduction

Benthic $\delta^{18}O$ stacks set benchmarks for comparison of paleoceanographic data (e.g., Ahn et al., 2017; Lisiecki & Raymo, 2005; Martinson et al., 1987) and are used to evaluate ice sheet evolution and climate responses to orbital forcing (e.g., Liautaud et al., 2020; Raymo et al., 2006; Tzedakis et al., 2017). The global "LR04" Plio-Pleistocene stack is one of the most commonly used benthic $\delta^{18}O$ stacks (Lisiecki & Raymo, 2005). Given its wide use, the accuracy of LR04, even in relatively minor details, has important implications for a broad range of paleoceanographic applications.

Wilkens et al. (2017) identified 1.8-1.9 Ma as a period where the LR04 stack differs significantly from a benthic $\delta^{18}O$ stack of five Ceara Rise cores. The Ceara Rise stack exhibits fewer glacial cycles compared to LR04 during 1.8-1.9 Ma, casting doubt on how globally representative LR04 was during the early Pleistocene. Wilkens et al. (2017) attributed the discrepancy to LR04's choice of the initial alignment target records, ODP (Ocean Discovery Program) sites 677 and 849. Sites 677 and 849 use splicing to construct continuous records from adjacent drill holes, a common practice for achieving complete recovery at ODP sites. Problems with splicing, Wilkens et al. contended, might have made sites 677 and 849 records inaccurate.

Several recent advances provide us with an opportunity to place in a broader context the discrepancy with LR04 found by Wilkens et al. (2017). First, newly developed software for stacking benthic $\delta^{18}O$ records requires fewer input records and enables us to efficiently construct regional stacks (Lee and Rand et al., 2023), which can reveal spatial variability that is otherwise masked in global stacks (Lisiecki & Raymo, 2009; Lisiecki & Stern, 2016; Skinner & Shackleton, 2005; Stern & Lisiecki, 2014). We can thus assess whether the pattern seen in the Ceara Rise stack is representative of regional or global changes. Second, the subsequent publication of higher-resolution Atlantic records, e.g., Hodell and Channell (2016), allows an investigation into the 1.8-1.9 Ma period with less ambiguity. Third, the observation of a Laurentide meltwater event during the 1.8-1.9 Ma period (Shakun et al., 2016) points to a potential mechanistic explanation for the Ceara Rise $\delta^{18}O$ signal identified by Wilkens et al. Here, we apply these new data and techniques to demonstrate that the 1.8-1.9 Ma period stands out as an unusual instance of regional divergence in Pleistocene benthic $\delta^{18}O$. We discuss the mechanisms that could have caused this divergence and implications for the LR04 stack.

Methods

We construct new Pleistocene regional Atlantic and Pacific Pleistocene stacks using 209 benthic $\delta^{18}O$ records, including 55 records from LR04 (Lisiecki & Raymo, 2005), 132 additional records from the ProbStack (Ahn et al., 2017), and 22 recently published records identified by this study (Table S1; Fig. S1-2). Many of the newly added records have relatively high resolutions, resulting in a 48% increase in data points compared to the ProbStack (Figs. S1-2). Over the Pleistocene, the Pacific stack includes data from 80 cores while the Atlantic stack includes data from 119 cores. To evaluate the hypothesis of Wilkens et al. (2017), we also construct shorter regional stacks for the Atlantic and the Pacific from 1.5 to 2.1 Ma. Between 1.8-1.9 Ma, there are 14 Pacific cores and 25 Atlantic cores. An Indian Ocean stack was not constructed because only one record is available from the Indian Ocean during 1.8-1.9 Ma.

The new stacks are created using Bayesian Inference Gaussian Process regression and Multiproxy Alignment for Continuous Stacks (BIGMACS), which is a newly developed software package for probabilistically stacking ocean sediment core data and constructing multiproxy age models (Lee and Rand et al., 2023). Unlike other probabilistic benthic $\delta^{18}O$ alignment software (Ahn et al., 2017; Lin et al., 2014), BIGMACS can reliably construct benthic $\delta^{18}O$ stacks using a smaller number of cores because it estimates a time-continuous signal using Gaussian process regression (Rasmussen & Williams, 2005). This enhances our ability to create and compare benthic $\delta^{18}O$ stacks for the Atlantic and the Pacific back to the early Pleistocene (see below). Another advancement of BIGMACS is that it probabilistically integrates additional depth-age estimates provided by the user.

BIGMACS stack construction requires an initial alignment target, for which we used the LR04 global stack (Lisiecki & Raymo, 2005). However, because the LR04 stack may not be a good representation of $\delta^{18}O$ variability from 1.8-1.9 Ma, its use as an initial alignment target could be problematic. For the 1.5-2.1 Ma stacks, we assigned additional age control points in BIGMACS for records that have sufficient resolution by visually identifying the glacial maxima associated

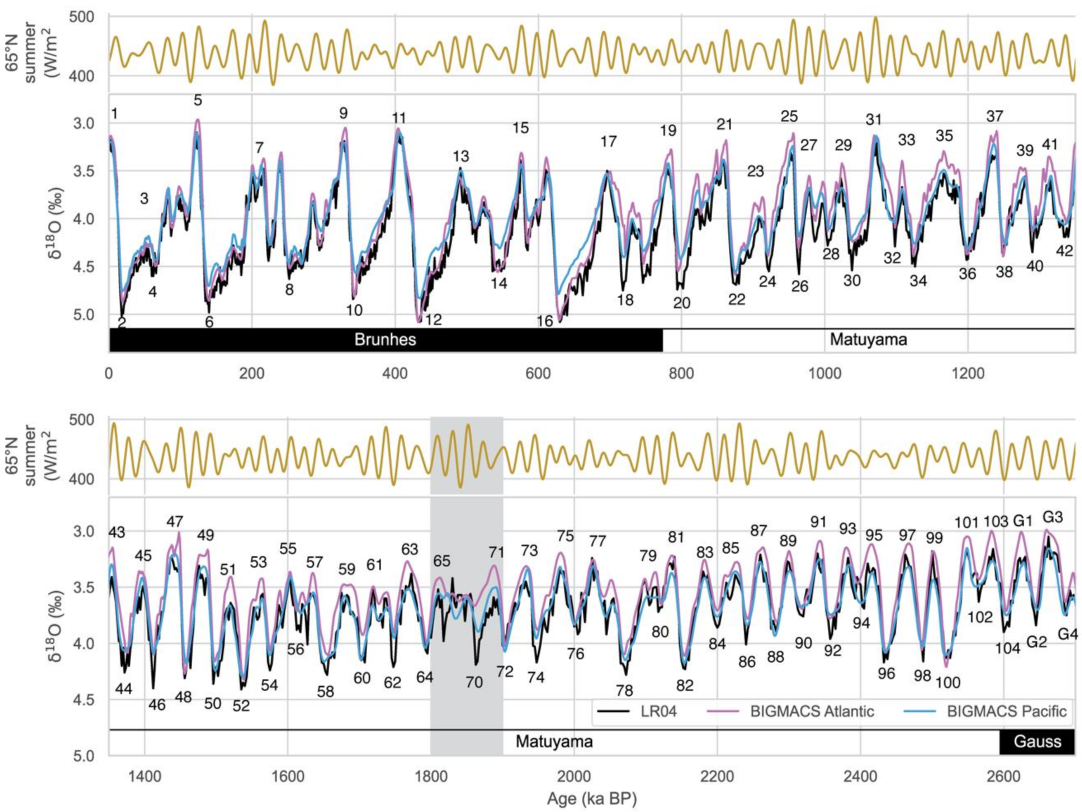

Figure 1. BIGMACS regional Pleistocene stacks for the Pacific (blue) and Atlantic (purple) without added tie points. The results presented are the stack means. Also shown is the LR04 global stack (black). The gray area is the 1.8-1.9 Ma period when the two BIGMACS regional stacks diverge. Also shown on top is the summer insolation at 65 °N. The numbers mark the Marine Isotope Stages. The black and white rectangles denote the geomagnetic chrons.

with MIS 64 and 74 and assigning them ages based on the respective obliquity minima (1.793 and 1.958 Ma). Because of the disagreement particularly between the LR04 global stack and

Atlantic records, we additionally identified the glacial maxima associated with MIS 68 and 70 in the Atlantic records that have sufficient resolution and assigned them as “additional ages” in BIGMACS based on the respective Northern Hemisphere (NH) insolation minima (1.841 and 1.864 Ma) with a 1-kyr standard deviation. (MIS 66 was not used because it was poorly defined in most high-resolution records.) In selecting these age constraints, we are guided by the average normalized sedimentation rate to ensure it is relatively steady and with no large deviations between tie points (Text S1, Fig. S3). We do not propose that these age assignments are necessarily appropriate corrections to the MIS ages of the LR04 stack; we merely use them to ensure consistent alignments in BIGMACS where fit to the original LR04 stack is poor. The discrepancies in the regional stacks between 1.8-1.9 Ma can also be seen in the full Pleistocene stacks for which we did not set any additional age controls (Text S2 and Fig. 1); however, the assigned age control points do affect the glacial-interglacial features of the regional stacks from 1.8-1.9 Ma (Fig. 2). Further details on the settings and parameters we used in BIGMACS are available (Text S2).

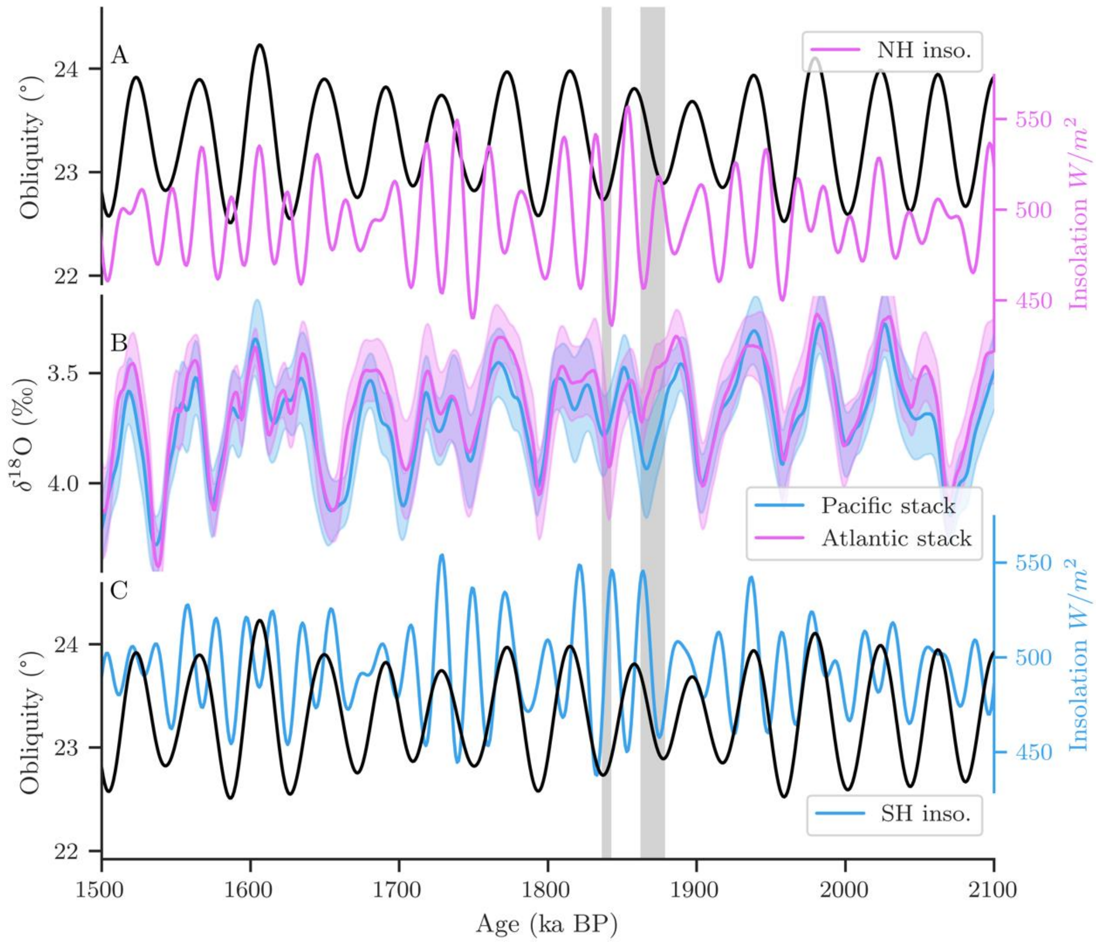

Figure 2. BIGMACS Atlantic and Pacific regional stacks compared to orbital parameters. (A) Obliquity (black) and summer insolation at 65°N (purple). The results presented are the stack means. (B) BIGMACS Atlantic (purple) and Pacific (blue) regional stacks. Shading denotes the 1σ uncertainty of the stack δ^{18}O values. (C) Obliquity (black) and summer insolation at 65°S (blue). The vertical gray shades associate glacial periods in the regional benthic δ^{18}O stacks with the corresponding orbital parameters.

Can we detect the same Atlantic-Pacific difference in the classic LR04 stack (Lisiecki & Raymo, 2005)? We separated the input records of LR04 based on ocean basins using the same δ^{18}O data on the age models used to construct the LR04 stack and binned at the same 2.5-kyr resolution used for the LR04 stack from 1.5-3 Ma. We refer to these results as the LR04 Atlantic/Pacific binned stacks.

Results

The new Pleistocene Atlantic and Pacific stacks, for the most part, closely follow each other except at a few places, notably during 1.8-1.9 Ma (Fig. 1). In the 1.5-2.1 Ma stacks with tie-point-guided alignments (Fig. 2), the glacial maximum at ~1.863 Ma (MIS 70) is much stronger in the Pacific than the Atlantic. In comparison to other glacial maxima from 1.5-2.1 Ma, the Atlantic benthic $\delta^{18}O$ response at MIS 70 more closely resembles a cold isotopic substage within a long interglacial than a glacial maximum. In contrast, the Atlantic stack's glacial maximum at ~1.841 Ma (MIS 68) is stronger than in the Pacific stack. The 1.5-2.1 Ma Atlantic stack differs substantially from both LR04 and ProbStack (Ahn et al., 2017) from 1.8-1.9 Ma, more closely resembling the Ceara Rise stack incorporated in CENOGRID (Wilkens et al., 2017; Westerhold et al., 2020) (Fig. S4). LR04 shows two poorly resolved glacial intervals (MIS 66 and 68) between two relatively normal glacial maxima (MIS 64 and 70); in contrast, the new Atlantic stack has a very weak MIS 70 while MIS 68 is similar in magnitude to MIS 64 and 72. However, marine isotope stages of the Pacific stack are similar to those in ProbStack from 1.8-1.9 Ma but with substantially smaller 95% confidence intervals. Another Atlantic-Pacific difference appears at ~2.05 Ma during the transition from glacial MIS 78 to interglacial MIS 77, during which the Atlantic stack shows a stronger interglacial substage (similar to LR04) than the Pacific stack.

Like the regional BIGMACS stacks, the LR04 Atlantic and Pacific binned stacks differ from one another between 1.8-1.9 Ma (Fig. S5). MIS 66 and 68 are absent in the LR04 Atlantic binned stack, whereas the Pacific binned stack matches LR04 well. Discrepancies in the relative amplitudes of MIS 68 and 70 between the Atlantic stacks produced by BIGMACS and LR04 binning may be caused by alignment errors during LR04 construction associated with relatively low-resolution Atlantic records. The new BIGMACS Atlantic stack contains more than double the $\delta^{18}O$ measurements of the LR04 Atlantic binned stack from 1.8-1.9 Ma.

Discussion

Stratigraphic implications

In all versions of the regional stacks we evaluated (with and without tie points), Atlantic benthic $\delta^{18}O$ exhibits a different pattern of variability than the Pacific between 1.8-1.9 Ma. Differences between regional stacks and the LR04 global stack at this time also provide a potential explanation for previous studies, including Wilkens et al. (2021), that found discrepancies with the LR04 stack between 1.8-1.9 Ma. For example, modeled ice volume differed more than normal from a benthic $\delta^{18}O$ record aligned to LR04 during 1.8-1.9 Ma (Liautaud et al., 2020 and Fig. 4b therein), probably because of distorted glacial cycles in the LR04 stack. A problem with the LR04 stack is also suggested by a divergence of ~30 kyr between tuned and untuned (depth-derived) age estimates for the LR04 stack from 1.8-1.9 Ma (Lisiecki, 2010 and Fig. S1 therein).

Regardless of the cause of the Atlantic-Pacific divergence, our results demonstrate that regional benthic $\delta^{18}O$ stacks are preferable to global stacks for age model development by stratigraphic alignment. The LR04 stack was created by performing pairwise alignment on all benthic $\delta^{18}O$ records to a target record. The targets were picked because of their relatively high resolution, low noise, and lack of apparent hiatuses. During 1.8-1.9 Ma, LR04 used two sites, ODP 677 and 849, to construct two stacks and observed that the resulting stack was largely independent of the target used. However, both sites 677 and 849 are from the Pacific, which our analysis show are quite dissimilar to Atlantic $\delta^{18}O$ records between 1.8-1.9 Ma. The poor fit between Atlantic records and the Pacific targets likely resulted in localized alignment errors for the Atlantic records.

The delicate task of choosing the right target cores for alignment is alleviated by the algorithmic approaches of HMM-Stack and BIGMACS (Ahn et al., 2017; Lee and Rand et al., 2023). These software packages align records to a target but iteratively update the alignment target to incorporate information from all other cores, thus reducing the reliance on the user-specified target. However, Atlantic and Pacific records were not analyzed separately when HMM-Stack was used to construct ProbStack. The iterative approach of BIGMACS was sufficient to identify a difference between the Atlantic and Pacific stacks without tie points (Fig. 1), but using the LR04 stack as our initial guess for the regional stacks resulted in ambiguous alignments and distortion of the glacial cycle features from 1.8-1.9 Ma. Ultimately, we bypassed this issue by manually defining several tie points for glacial maxima between 1.79-1.96 Ma for the benthic $\delta^{18}O$ records in which the glacial maxima could be confidently identified (Fig. S6).

Mechanisms for generating benthic $\delta^{18}O$ gradients in the 41-kyr world

Although benthic $\delta^{18}O$ is often considered a well-mixed proxy for global ice volume, one possible explanation for the regional difference in benthic $\delta^{18}O$ from 1.8-1.9 Ma may be differences in the deep water temperature or salinity of the two ocean basins. The modern global ocean mixing time of oxygen isotopes is about 1500 years (Broecker & Peng, 1983; Rohling, 2013), which is too short to explain gradients in seawater $\delta^{18}O$ that persist on orbital timescales (Morée et al., 2021). In contrast, regional variations in benthic $\delta^{18}O$ values associated with differences in deep water temperature or salinity may persist over tens of thousands of years. For example, regional differences observed in the amplitude of benthic $\delta^{18}O$ change during the last interglacial period (MIS 5) are most easily interpreted as temperature or salinity gradients between deep water masses (Lisiecki & Stern, 2016). During the 41-kyr world, the amplitude of global ice volume change is smaller in magnitude such that potential regional gradients in deep water temperature or salinity might constitute a larger percentage of the benthic $\delta^{18}O$ signal.

Benthic $\delta^{18}O$ values recorded for Pacific Deep Water (PDW) and North Atlantic Deep Water (NADW) could differ if the temperature or salinity the two water masses exhibited sensitivity to different forcings. For example, Raymo et al. (2006) asserted that the temperature/salinity of the Southern Ocean likely co-varied with the changes in the Antarctic ice volume; such Southern Ocean changes would also be expected to affect Antarctic Bottom Water (AABW) and PDW. At the same time, the NADW temperature or salinity signal would likely have changed concurrently with NH ice sheet dynamics (Marcott et al., 2011).

Circulation reconstructions for the 41-kyr world are consistent with deep water in the Atlantic and Pacific responding to different hemispheric insolation forcing between 1.8-1.9 Ma. The 41-kyr world Atlantic was primarily under the influence of the northern-sourced water, which filled most of the mid-depth to deep Atlantic, while southern-sourced water occasionally occupied the bottom depths (Cronin et al., 1996; Jakob et al., 2021; Lang et al., 2016; Zhang et al., 2013). Although the 41-kyr world Pacific might have seen deep water formation in the subarctic North Pacific (Burls et al., 2017; Ford et al., 2022), this northern-sourced Pacific deep water was limited to depths shallower than 3000 m. Antarctic-sourced bottom water is thought to have filled the deep Pacific below 3000 m (Burls et al., 2017; Ford et al., 2022), the depths from which most high-resolution Pacific cores in our compilation were recovered. The only two high-resolution Pacific cores in our compilation retrieved from sites shallower than 3000 m, ODP 1143 and 1241, display different benthic $\delta^{18}O$ patterns than the deeper cores (Figs. S6 and S8), possibly due to the influence of NPDW.

We tentatively attribute the regional benthic $\delta^{18}O$ divergence to the effects of deep water temperature and/or salinity because we are unable to differentiate the impacts of temperature and salinity using only benthic $\delta^{18}O$. One bottom water temperature record from the Atlantic suggests that deep water temperature and benthic $\delta^{18}O$ co-vary during 1.8-1.9 Ma (Sosdian & Rosenthal, 2009), possibly hinting at the important influence of bottom water temperature on Atlantic benthic $\delta^{18}O$ during this period. As far as we are aware, there is not a commensurate Pacific deep water temperature record that can resolve glacial-interglacial cycles during 1.8-1.9 Ma. Such a record could shed more light on the role deep water temperature played in the Atlantic-Pacific divergence in benthic $\delta^{18}O$ records.

Antiphased Precession Effects between 1.8-1.9 Ma

Although orbital insolation is consistently dominated by precession (Fig. 3), benthic $\delta^{18}O$ records exhibit strong 41-kyr obliquity cycles during the late Pliocene/early Pleistocene. This mismatch between the substantial role that precession played in modulating the NH summer insolation and the apparent lack of a precessional imprint in geological records is termed the "41-kyr problem" (Raymo & Nisancioglu, 2003; Watanabe et al., 2023). Many researchers have put forward theories on why the 41-kyr world is dominated by obliquity. Among them, the Antiphase Hypothesis has particular appeal to explain our observations (Morée et al., 2021; Raymo et al., 2006). The Antiphase Hypothesis proposes that opposing responses of the northern and southern hemisphere ice sheets on precessional time scales canceled each other out in the global ice volume signal. For example, while cool NH summers lead to northern ice growth, coeval warm Southern Hemisphere (SH) summers act to shrink the Antarctic Ice Sheet. Obliquity, which exerts a symmetric effect on both hemispheres, is left as the governing cyclicity of global ice volume during this period.

The Antiphase Hypothesis provides a framework to explain the Atlantic-Pacific difference in benthic $\delta^{18}O$ records during 1.8-1.9 Ma (Fig. 2). While obliquity still paces the glacial-interglacial cycles in global ice volume, the opposite phase of the northern and southern hemisphere insolation on precession time scales could have influenced the magnitudes of glacial benthic $\delta^{18}O$ change in the Atlantic and the Pacific. In particular, the 1.8-1.9 Ma time interval experienced uniquely strong precession and weak obliquity relative to the rest of the 41-kyr world (Fig. 3). While high-latitude summer insolation is always dominated by precession (Raymo & Nisancioglu, 2003), the contrast between the strong precession and weak obliquity during 1.8-1.9 Ma stands out. Other times of similar relative power of obliquity and precession forcing are not directly comparable because they occur before or after the 41-kyr world, e.g., 0.9-1 Ma and 3-3.1 Ma. Before the 41-kyr world, the northern hemisphere was largely ice-free (Sosdian & Rosenthal, 2009). After the 41-kyr world, the Laurentide ice sheet expanded in size and the glacial cycles transitioned to 100-kyr pacing (Lisiecki & Raymo, 2007). The 1.8-1.9 Ma period is, thus, a unique window of time when more precession response might be expected compared to the rest of the 41-kyr world.

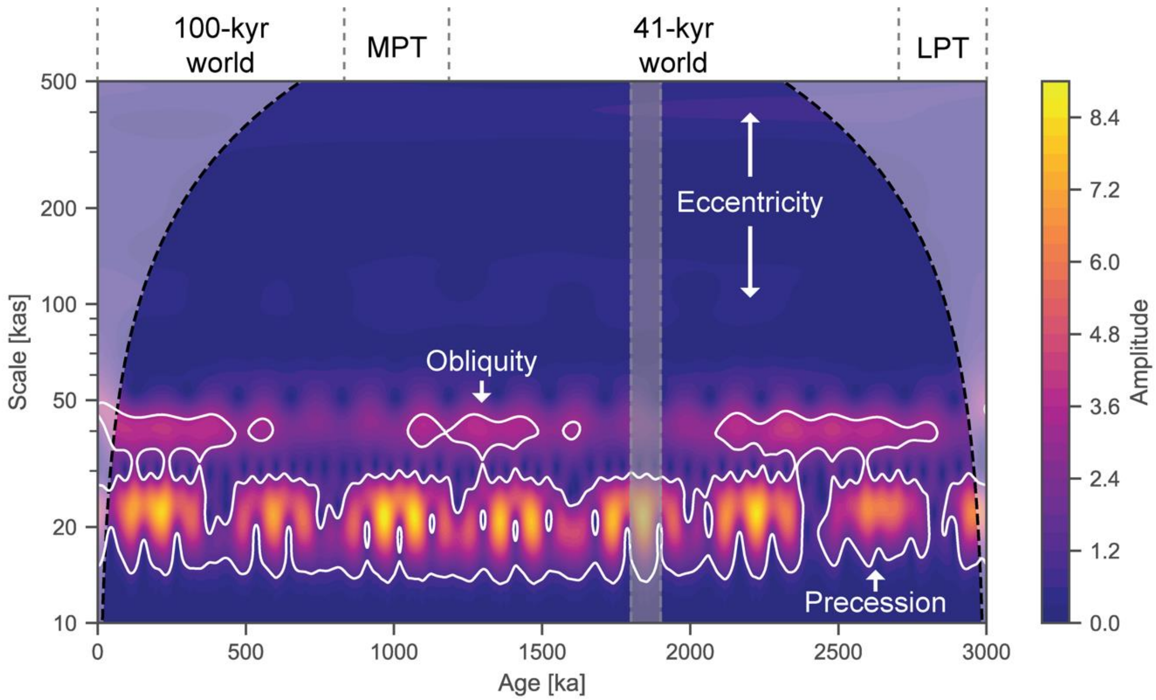

Figure 3. Wavelet spectrum of insolation at 65° N for the Plio-Pleistocene generated with Wavelet Continuous Transform using the Morlet wavelet (Torrence and Compo, 1998). The white lines delineate regions of the spectrum that are significant against a random AR(1) benchmark. The dashed lines denote the 1.8-1.9 Ma period where the Atlantic and Pacific records records diverge. LPT: Late Pliocene Transition (Sosdian and Rosenthal, 2009). MPT: Mid-Pleistocene Transition. This figure was generated with Pyleoclim (Khider et al., 2022).

Examining the northern and southern summer insolation forcing from 1.8-1.9 Ma (Fig. 2), we find that the magnitudes of the Atlantic and Pacific glacial responses are likely caused by the hemispheric insolation differences during the obliquity minima. The obliquity minimum at 1.878 Ma coincided with a maximum in NH summer insolation and minimum SH summer insolation due to the opposite hemispheric effects of precession on seasonal insolation. The Southern Ocean and PDW would be expected to cool strongly during MIS 70 because SH insolation is low during the obliquity minimum. In contrast, moderately high NH insolation would produce a weaker and delayed glacial response for MIS 70 in northern hemisphere climate and NADW. By the time NH summer insolation reaches its minimum, obliquity is relatively high and would quickly reverse the NH cooling trend. Hemispheric circumstances are reversed during MIS 68 with NH summer insolation low early during the obliquity minimum (amplifying NH/NADW cooling) while Southern Ocean/PDW cooling is delayed by a SH insolation peak, which would initially suppress SH cooling. However, because the SH insolation minimum was not as far offset from the obliquity minimum during MIS 68 as the NH insolation was during MIS 70, the antiphase insolation effect is weaker for MIS 68.

Notably, Atlantic $\delta^{18}O$ responses are similar for MIS 70 and MIS 56 at ~1.6 Ma (Fig. 2). They are similarly weak glacials and both have NH precession maxima that coincide with obliquity minima. The interesting difference between the two glacials is that the Pacific $\delta^{18}O$ response matches the Atlantic during MIS 56, in contrast to the strong Pacific glacial maximum during MIS 70. The discrepancy in Atlantic-Pacific divergence could be because MIS 70 has stronger precession forcing and weaker obliquity than MIS 56. Thus, the relatively strong power of precession forcing from 1.8-1.9 Ma may account for the greater regional benthic $\delta^{18}O$ difference during this time compared to the rest of the 41-kyr world, leaving vestiges of precession-driven regional temperature/salinity signals in the otherwise obliquity-dominated global ice volume component of benthic $\delta^{18}O$.

Another potential impact of strong precession forcing during the 1.8-1.9 Ma period is a Laurentide meltwater event in the Gulf of Mexico similar to or even larger in magnitude than those in the late Pleistocene (Shakun et al., 2016). Alignment of the Gulf of Mexico core which records this meltwater event to our Atlantic stack (Fig. S6, bottom panel) suggests that the event occurred during MIS 71, immediately before the very weak glacial maximum in the Atlantic. Terrestrial deposits along the Mississippi River dated to 1.8-2.0 Ma additionally substantiate the size and timing of this Gulf of Mexico meltwater drainage event (Rovey II & Spoering, 2020), indicating a rapid loss of Laurentide ice similar to meltwater events during the last deglaciation (Barber et al., 1999; Tarasov & Peltier, 2005). As this early Pleistocene meltwater event coincides with one of the weakest obliquity maxima of the 41-kyr world, it suggests sensitivity of the Laurentide ice sheet to the strong precession forcing at this time. Additionally, the meltwater event may have directly or indirectly contributed to the weaker Atlantic benthic $\delta^{18}O$ response during MIS 70. For example, the large meltwater input to the North Atlantic could have slowed deep water mixing times between the Atlantic and Pacific relative to their average for the 41-kyr world, prolonging the Atlantic-Pacific benthic $\delta^{18}O$ contrast. The weak Atlantic benthic $\delta^{18}O$ response during MIS 70 could also be accentuated by dissolution of benthic foraminiferal calcite in the Atlantic if the preceding meltwater event prolonged the residence time of North Atlantic Deep Water; however, dissolution is unlikely to fully account for the Atlantic-Pacific discrepancy (Text S3).

Our assertion that precession, in addition to obliquity, affects the 41-kyr world glacial cycles joins an array of previous studies reaching similar conclusions. An early study observed an increased response to precession in benthic $\delta^{18}O$ beginning at ~2.5 Ma (Lisiecki & Raymo, 2007). Another study detected a nontrivial precession contribution to benthic $\delta^{18}O$ variability from 1-3 Ma using Empirical Nonlinear Orbital Fitting (Liautaud et al., 2020). More recently, precession influence during the 41-kyr world has been shown in sedimentary elemental records (Sun et al., 2021), sea level (Vaucher et al., 2021), ice-rafted debris (Barker et al., 2022), and ice sheet modeling (Watanabe et al., 2023). Compared to the existing evidence, our finding suggests that between 1.8-1.9 Ma benthic $\delta^{18}O$ – the data originally used to demonstrate the “41-kyr problem” (Raymo & Nisancioglu, 2003) – responds to precession forcing differently depending on geographical locations, likely due to the different source regions of deep water masses.

Conclusion

Benthic $\delta^{18}O$ from five Ceara Rise sites was previously shown to differ from the LR04 global benthic $\delta^{18}O$ stack between 1.8-1.9 Ma (Wilkens et al., 2017). Our investigation reveals that discrepancy with the LR04 stack is widespread over this time interval; most Atlantic $\delta^{18}O$ records show a different pattern of Marine Isotope Stages than Pacific $\delta^{18}O$ records during 1.8-1.9 Ma. The largest difference between the Atlantic and Pacific benthic $\delta^{18}O$ stacks occurs during MIS 70 at ~1.878 Ma, and 1.8-1.9 Ma is the only portion of the Pleistocene for which glacial cycles in the regional stacks differ substantially from LR04 (Fig. 1). The next largest regional difference is an isotopic substage between MIS 77 and 78 at ~2.05 Ma that is isotopically lighter (or warmer) in the Atlantic than the Pacific. Throughout the rest of the Pleistocene, the Atlantic and Pacific regional stacks agree with LR04 and ProbStack (Fig. 1).

A re-examination of the Pacific alignment targets used in the LR04 construction process from 1.8-1.9 Ma explains why the LR04 stack more closely resembles the Pacific records and produced misalignments of the Atlantic records. This example demonstrates why regional benthic $\delta^{18}O$ stacks are preferable to global stacks for age model development by stratigraphic alignment. The new stacking software BIGMACS facilitates construction of regional stacks by requiring fewer records to generate a stack, but it still has some sensitivity to the choice of initial alignment target. The regional stacks presented here have largely inherited the orbitally tuned age model of the LR04 stack, and updated regional age models, particularly from 1.8-1.9 Ma, should be developed based on analysis of the regional stacks.

We propose that the cause of the Atlantic-Pacific divergence from 1.8-1.9 Ma is hemispheric sensitivity to antiphased precession forcing, specifically that Atlantic benthic $\delta^{18}O$ at this time was more sensitive to NH summer insolation while deep Pacific benthic $\delta^{18}O$ was more sensitive to SH summer insolation. This benthic $\delta^{18}O$ discrepancy could be caused by variations in the temperature or salinity of northern- versus southern-source deep water rather than requiring uneven mixing of meltwater inputs. The unusually strong precession power and weak obliquity power of orbital cycles from 1.8-1.9 Ma and a contemporaneous meltwater event in the Gulf of Mexico lend support to the Antiphase Hypothesis as a possible mechanism to explain spatial variability in benthic $\delta^{18}O$ during this portion of the 41-kyr world. Our study joins a variety of others (Barker et al., 2022; Liautaud et al., 2020; Lisiecki & Raymo, 2007; Sun et al., 2021; Vaucher et al., 2021; Watanabe et al., 2023) suggesting that precession, in addition to obliquity, plays a role in pacing climate signals during the 41-kyr world.

Acknowledgements
This study benefited from discussions with Devin Rand and Bethany Hobart. This research was funded in part by the Heising-Simons Foundation grant number 2021–2799. Use was made of computational facilities purchased with funds from the National Science Foundation (CNS-1725797) and administered by the Center for Scientific Computing (CSC). The CSC is supported by the California NanoSystems Institute and the Materials Research Science and Engineering Center (MRSEC; NSF DMR 2308708) at UC Santa Barbara. We also acknowledge high-performance computing support from Casper (doi:10.5065/D6RX99HX) provided by NCAR's Computational and Information Systems Laboratory, sponsored by the National Science Foundation.

Availability Statement
The BIGMACS stacking software is available at https://github.com/eilion/BIGMACS. The compiled benthic $\delta^{18}O$ records and the resulting regional stacks will be available upon publication in a Figshare repository or upon request during the review process.

References

Ahn, S., Khider, D., Lisiecki, L. E., & Lawrence, C. E. (2017). A probabilistic Pliocene–Pleistocene stack of benthic $\delta^{18}O$ using a profile hidden Markov model. *Dynamics and Statistics of the Climate System*, *2*(1). https://doi.org/10.1093/climsys/dzx002

Barber, D. C., Dyke, A., Hillaire-Marcel, C., Jennings, A. E., Andrews, J. T., Kerwin, M. W., et al. (1999). Forcing of the cold event of 8,200 years ago by catastrophic drainage of Laurentide lakes. *Nature*, *400*(6742), 344–348. https://doi.org/10.1038/22504

Barker, S., Starr, A., van der Lubbe, J., Doughty, A., Knorr, G., Conn, S., et al. (2022). Persistent influence of precession on northern ice sheet variability since the early Pleistocene. *Science*, *376*(6596), 961–967. https://doi.org/10.1126/science.abm4033

Broecker, W. S., & Peng, T.-H. (1983). *Tracers in the sea*. https://doi.org/10.1016/0016-7037(83)90075-3

Burls, N. J., Fedorov, A. V., Sigman, D. M., Jaccard, S. L., Tiedemann, R., & Haug, G. H. (2017). Active Pacific meridional overturning circulation (PMOC) during the warm Pliocene. *Science Advances*, *3*(9), e1700156. https://doi.org/10.1126/sciadv.1700156

Cronin, T. M., Raymo, M. E., & Kyle, K. P. (1996). Pliocene (3.2–2.4 Ma) ostracode faunal cycles and deep ocean circulation, North Atlantic Ocean. *Geology*, *24*(8), 695–698. https://doi.org/10.1130/0091-7613(1996)024<0695:PMOFCA>2.3.CO;2

Ford, H. L., Burls, N. J., Jacobs, P., Jahn, A., Caballero-Gill, R. P., Hodell, D. A., & Fedorov, A. V. (2022). Sustained mid-Pliocene warmth led to deep water formation in the North Pacific. *Nature Geoscience*, *15*(8), 658–663. https://doi.org/10.1038/s41561-022-00978-3

Hodell, D. A., & Channell, J. E. T. (2016). Mode transitions in Northern Hemisphere glaciation: co-evolution of millennial and orbital variability in Quaternary climate. *Climate of the Past*, *12*(9), 1805–1828. https://doi.org/10.5194/cp-12-1805-2016

Jakob, K. A., Pross, J., Link, J. M., Blaser, P., Hauge Braaten, A., & Friedrich, O. (2021). Deep-ocean circulation in the North Atlantic during the Plio-Pleistocene intensification of Northern Hemisphere Glaciation (~2.65–2.4 Ma). *Marine Micropaleontology*, *165*, 101998. https://doi.org/10.1016/j.marmicro.2021.101998

Khider, D., Emile-Geay, J., Zhu, F., James, A., Landers, J., Ratnakar, V., & Gil, Y. (2022). Pyleoclim: Paleoclimate Timeseries Analysis and Visualization With Python. *Paleoceanography and Paleoclimatology*, *37*(10), e2022PA004509. https://doi.org/10.1029/2022PA004509

Lang, D. C., Bailey, I., Wilson, P. A., Chalk, T. B., Foster, G. L., & Gutjahr, M. (2016). Incursions of southern-sourced water into the deep North Atlantic during late Pliocene glacial intensification. *Nature Geoscience*, *9*(5), 375–379. https://doi.org/10.1038/ngeo2688

Lee, T., Rand, D., Lisiecki, L. E., Gebbie, G., & Lawrence, C. (2023). Bayesian age models and stacks: combining age inferences from radiocarbon and benthic $\delta^{18}O$ stratigraphic alignment. *Climate of the Past*, *19*(10), 1993–2012. https://doi.org/10.5194/cp-19-1993-2023

Liautaud, P. R., Hodell, D. A., & Huybers, P. J. (2020). Detection of significant climatic precession variability in early Pleistocene glacial cycles. *Earth and Planetary Science Letters*, *536*, 116137. https://doi.org/10.1016/j.epsl.2020.116137

Lin, L., Khider, D., Lisiecki, L. E., & Lawrence, C. E. (2014). Probabilistic sequence alignment of stratigraphic records. *Paleoceanography*, *29*(10), 976–989. https://doi.org/10.1002/2014PA002713

Lisiecki, L. E. (2010). Links between eccentricity forcing and the 100,000-year glacial cycle. *Nature Geoscience*, *3*(5), 349–352. https://doi.org/10.1038/ngeo828

Lisiecki, L. E., & Raymo, M. E. (2005). A Pliocene-Pleistocene stack of 57 globally distributed benthic $\delta^{18}O$ records. *Paleoceanography*, *20*(1), 1–17. https://doi.org/10.1029/2004PA001071

Lisiecki, L. E., & Raymo, M. E. (2007). Plio–Pleistocene climate evolution: trends and transitions in glacial cycle dynamics. *Quaternary Science Reviews*, *26*(1), 56–69. https://doi.org/10.1016/j.quascirev.2006.09.005

Lisiecki, L. E., & Raymo, M. E. (2009). Diachronous benthic δ18O responses during late Pleistocene terminations. *Paleoceanography*, *24*(3). https://doi.org/10.1029/2009PA001732

Lisiecki, L. E., & Stern, J. V. (2016). Regional and global benthic δ18O stacks for the last glacial cycle. *Paleoceanography*, *31*(10), 1368–1394. https://doi.org/10.1002/2016PA003002

Marcott, S. A., Clark, P. U., Padman, L., Klinkhammer, G. P., Springer, S. R., Liu, Z., et al. (2011). Ice-shelf collapse from subsurface warming as a trigger for Heinrich events. *Proceedings of the National Academy of Sciences*, *108*(33), 13415–13419. https://doi.org/10.1073/pnas.1104772108

Martinson, D. G., Pisias, N. G., Hays, J. D., Imbrie, J., Moore, T. C., & Shackleton, N. J. (1987). Age Dating and the Orbital Theory of the Ice Ages: Development of a High-Resolution 0 to 300,000-Year Chronostratigraphy. *Quaternary Research*, *27*(1), 1–29. https://doi.org/10.1016/0033-5894(87)90046-9

Morée, A. L., Sun, T., Bretones, A., Straume, E. O., Nisancioglu, K., & Gebbie, G. (2021). Cancellation of the Precessional Cycle in δ18O Records During the Early Pleistocene.

Geophysical Research Letters, *48*(3), e2020GL090035. https://doi.org/10.1029/2020GL090035

Rasmussen, C. E., & Williams, C. K. I. (2005). *Gaussian Processes for Machine Learning*. Cambridge: MIT Press.

Raymo, M. E., & Nisancioglu, K. H. (2003). The 41 kyr world: Milankovitch's other unsolved mystery. *Paleoceanography*, *18*(1). https://doi.org/10.1029/2002PA000791

Raymo, M. E., Lisiecki, L. E., & Nisancioglu, K. H. (2006). Plio-Pleistocene Ice Volume, Antarctic Climate, and the Global δ18O Record. *Science*, *313*(5786), 492–495. https://doi.org/10.1126/science.1123296

Rohling, E. J. (2013). Oxygen isotope composition of seawater. In *The Encyclopedia of Quaternary Science* (Vol. 2, pp. 915–922). Amsterdam: Elsevier.

Rovey II, C. W., & Spoering, G. (2020). Age and provenance of upland gravels in Missouri, USA, and their relationship to Early Pleistocene glaciation. *Boreas*, *49*(2), 333–349. https://doi.org/10.1111/bor.12429

Shakun, J. D., Raymo, M. E., & Lea, D. W. (2016). An early Pleistocene Mg/Ca-δ18O record from the Gulf of Mexico: Evaluating ice sheet size and pacing in the 41-kyr world. *Paleoceanography*, *31*(7), 1011–1027. https://doi.org/10.1002/2016PA002956

Skinner, L. C., & Shackleton, N. J. (2005). An Atlantic lead over Pacific deep-water change across Termination I: implications for the application of the marine isotope stage stratigraphy. *Quaternary Science Reviews*, *24*(5), 571–580. https://doi.org/10.1016/j.quascirev.2004.11.008

Sosdian, S., & Rosenthal, Y. (2009). Deep-Sea Temperature and Ice Volume Changes Across the Pliocene-Pleistocene Climate Transitions. *Science*, *325*(5938), 306–310. https://doi.org/10.1126/science.1169938

Stern, J. V., & Lisiecki, L. E. (2014). Termination 1 timing in radiocarbon-dated regional benthic δ^{18} O stacks: Regional benthic δ18O stacks. *Paleoceanography*, *29*(12), 1127–1142. https://doi.org/10.1002/2014PA002700

Sun, Y., McManus, J. F., Clemens, S. C., Zhang, X., Vogel, H., Hodell, D. A., et al. (2021). Persistent orbital influence on millennial climate variability through the Pleistocene. *Nature Geoscience*, 1–7. https://doi.org/10.1038/s41561-021-00794-1

Tarasov, L., & Peltier, W. R. (2005). Arctic freshwater forcing of the Younger Dryas cold reversal. *Nature*, *435*(7042), 662–665. https://doi.org/10.1038/nature03617

Torrence, C., & Compo, G. P. (1998). A practical guide to wavelet analysis. *Bull. Am. Meteor. Soc.*, *79*(1), 61–78. https://doi.org/10.1175/1520-0477(1998)079<0061:APGTWA>2.0.CO;2

Tzedakis, P. C., Crucifix, M., Mitsui, T., & Wolff, E. W. (2017). A simple rule to determine which insolation cycles lead to interglacials. *Nature*, *542*(7642), 427–432. https://doi.org/10.1038/nature21364

Vaucher, R., Dashtgard, S. E., Horng, C.-S., Zeeden, C., Dillinger, A., Pan, Y.-Y., et al. (2021). Insolation-paced sea level and sediment flux during the early Pleistocene in Southeast Asia. *Scientific Reports*, *11*(1), 16707. https://doi.org/10.1038/s41598-021-96372-x

Watanabe, Y., Abe-Ouchi, A., Saito, F., Kino, K., O'ishi, R., Ito, T., et al. (2023). Astronomical forcing shaped the timing of early Pleistocene glacial cycles. *Communications Earth & Environment*, *4*(1), 1–11. https://doi.org/10.1038/s43247-023-00765-x

Westerhold, T., Marwan, N., Drury, A. J., Liebrand, D., Agnini, C., Anagnostou, E., et al. (2020). An astronomically dated record of Earth's climate and its predictability over the last 66 million years. *Science*, *369*(6509), 1383–1387. https://doi.org/10.1126/science.aba6853

Wilkens, R. H., Westerhold, T., Drury, A. J., Lyle, M., Gorgas, T., & Tian, J. (2017). Revisiting the Ceara Rise, equatorial Atlantic Ocean: isotope stratigraphy of ODP Leg 154 from 0 to 5 Ma. *Climate of the Past*, *13*(7), 779–793. https://doi.org/10.5194/cp-13-779-2017

Zhang, Z.-S., Nisancioglu, K. H., Chandler, M. A., Haywood, A. M., Otto-Bliesner, B. L., Ramstein, G., et al. (2013). Mid-pliocene Atlantic Meridional Overturning Circulation not unlike modern. *Climate of the Past*, *9*(4), 1495–1504. https://doi.org/10.5194/cp-9-1495-2013

Geophysical Research Letters

Supporting Information for

Regional benthic $\delta^{18}O$ stacks for the "41-kyr world" - an Atlantic-Pacific divergence between 1.8-1.9 Ma

Yuxin Zhou[1], Lorraine E. Lisiecki[1], Taehee Lee[2], Geoffrey Gebbie[3], and Charles Lawrence[2]
[1]Department of Earth Science, University of California, Santa Barbara.
[2]Division of Applied Mathematics, Brown University.
[3]Physical Oceanography Department, Woods Hole Oceanographic Institution.

Contents of this file

Text S1 to S4
Figures S1 to S9
Tables S1

Text S1 – Basin-wide average normalized sedimentation rate

Over the Pleistocene, we can expect the global average normalized sedimentation rate to be fairly constant (Lisiecki & Raymo, 2005). We monitor the normalized sedimentation rate of our regional stacks when choosing additional age controls (i.e., tie points). To calculate the normalized sedimentation rate, each core's sedimentation rate based on BIGMACS alignment is divided by its mean sedimentation rate, interpolated to 1-kyr intervals, and averaged across all Atlantic or Pacific cores.

Text S2 – BIGMACS stack construction

In addition to the 1.5-2.1 Ma regional stacks discussed in the main text, we also constructed regional Pleistocene (0-2.7 Ma) stacks for the Atlantic and the Pacific. The construction of these stacks did not involve additional age controls except those identified from the Neptune database (see main text). Because of the intense computational resources required quickly exceed that of even a supercomputer (over 1 TB of RAM), both the Atlantic and the Pacific stacks were constructed in two segments (0-700 ka and 700-2700 ka for the Atlantic; 0-300 ka and 300-2700 ka for the Pacific). The time length of the segments during the more recent past is shorter because more $\delta^{18}O$ records are available, requiring a shorter interval of alignment to keep the use of computational resources reasonable. The overlaps between segments are averaged in stitching together the segments to create a stack for the entire Pleistocene.

BIGMACS stack construction requires an initial alignment target for the initial alignment all of the records, and we used the LR04 global stack (Lisiecki & Raymo, 2005). The software then iteratively updates the stack to which the records are aligned until convergence. We used the default settings for all the hyperparameters (Lee et al., 2023). The stack construction process also includes core-specific shift and scale parameters that are learned during the alignment using the Baum-Welch Expectation Maximization algorithm.

In constructing the new BIGMACS stacks, we incorporate age estimates from the Neptune Sandbox Berlin (NSB) database (Renaudie et al., 2020), which compiled biostratigraphic and paleomagnetic events from the International Ocean Discovery Program (IODP) and its predecessors. The conversion of NSB hole-specific meters below sea floor (mbsf) depths to meters composite depth (mcd) was done using the IODP Janus Depth Point Calculator. Because the age information provided by the NSB database does not come with uncertainty estimates, we conservatively specify the age uncertainty as Gaussian distributions with a standard deviation of 100 kyr. Due to the large uncertainty for these age constraints, the Atlantic and Pacific stacks mostly follow the age model of the LR04 stack used for the initial alignment target.

Text S3 – Alternative causes of regional divergence

Could the regional divergence be solely caused by the light $\delta^{18}O$ input into the Atlantic from the meltwater event alone? We do not find this explanation likely. First, the more recent meltwater events of the last glacial period led to only modest and relatively short-lived differences (4 kyr or less) between regional benthic $\delta^{18}O$ stacks (Lisiecki & Stern, 2016). In contrast, the glacial maximum in the Atlantic stack at 1.878 Ma, is barely identifiable and would probably require a meltwater event of much larger magnitude and duration. Second, Shakun et al. (2016) identified other meltwater events that do not produce the same regional divergences. The meltwater events other than the one at ~1.85 Ma (and possibly another at ~2.05 Ma) are not associated with clear differences in the Atlantic and Pacific benthic $\delta^{18}O$ records and have magnitudes both greater and smaller than the one at 1.85 Ma. Nevertheless, the meltwater event at 1.85 Ma and the associated light $\delta^{18}O$ input could have been a secondary contributing factor that led to the regional benthic $\delta^{18}O$ differences.

An alternative explanation for the Atlantic-Pacific divergence is that the meltwater event led to a foraminifera-barren zone in the Atlantic – a hiatus in the Atlantic benthic $\delta^{18}O$ records that left one or more marine isotope stages unrecorded. For example, foraminifera-barren zones in sediments are observed during Heinrich events of the last glacial cycle (Ruddiman & McIntyre 1981; Broecker et al. 1992; McManus et al. 1998) and the penultimate glaciation (Ruddiman et al. 1980). During these Heinrich events, icebergs and the accompanying meltwater were rapidly discharged into the North Atlantic from the Hudson Strait region during periods of Laurentide Ice Sheet instability (Heinrich 1998; Broecker et al. 1992; Zhou et al., 2021).

However, we find this explanation to be unlikely. While foraminifera dissolution may be an appealing explanation for the Atlantic-Pacific divergence we observed, we do not find a gap in benthic $\delta^{18}O$ measurements at this time or an apparent decrease in Atlantic sedimentation rates during this period (see Fig. S7 for an example using U1308). If a sedimentation hiatus in the Atlantic was responsible for failing to record the majority of a glacial period, we would expect a more discernable drop in the apparent Atlantic sedimentation rates between 1.8-1.9 Ma. If foraminifera dissolution played a role in causing the Atlantic-Pacific benthic $\delta^{18}O$ differences, that role is likely a minor one.

Text S4 – Visual confirmation of BIGMACS record alignment

To verify the Atlantic-Pacific difference identified by BIGMACS in record alignment, we developed a strategy to visually confirm the BIGMACS results for certain high-resolution cores during 1.8-1.9 Ma. While most of the glacial cycles in the 41-kyr world repeat the typical sawtooth pattern (gradual buildup and fast termination of ice sheets), some glacial cycles stand out with "double interglacial" or "step interglacial" features. Double interglacials are two interglacial periods interrupted by a weak and short glacial, structurally similar to Marine Isotope Stage 7 in the 100-kyr world (Choudhury et al., 2020). Step interglacials are similar to double interglacials in that two interglacials are interrupted by a weak and short glacial. However, unlike the double interglacials, the step interglacials start with a moderate interglacial followed by a second, comparatively more intense interglacial. The step interglacials represent a two-step transition that is similar to Marine Isotope Stage 13 in the 100-kyr world. The double interglacials and step interglacials before or after 1.8-1.9 Ma can serve as anchor points to contradict or corroborate the algorithmic alignment by BIGMACS during 1.8-1.9 Ma (Fig. S6).

The double interglacials during MIS 61 (~1.725 Ma) and the step interglacials during MIS 77 (~2.025 Ma) serve as useful anchors that can help visually confirm the BIGMACS alignment during 1.8-1.9 Ma (Fig. S6). Between MIS 61 and 1.8 Ma, benthic $\delta^{18}O$ records with sufficient resolution show one climatic cycle. Between MIS 77 and 1.9 Ma, benthic $\delta^{18}O$ records show two climatic cycles. As a result, we have added confidence in the BIGMACS record alignment during 1.8-1.9 Ma. Any discrepancy among records during this period is hard to dismiss as erroneous algorithmic alignment.

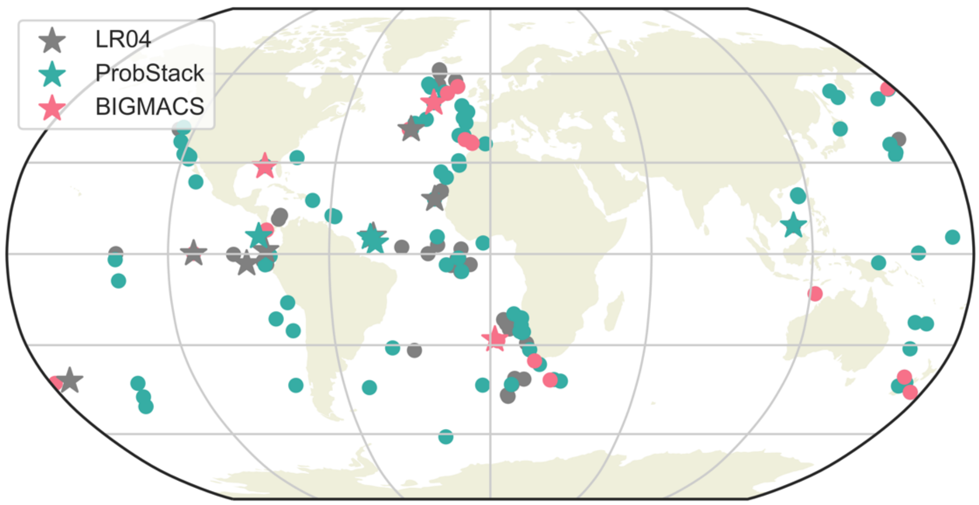

Figure S1. Map of the input cores for the BIGMACS Atlantic and Pacific stacks construction, including existing compilations and additional records newly compiled for this study. Stars mark the high-resolution cores shown in Fig. S3 and S4.

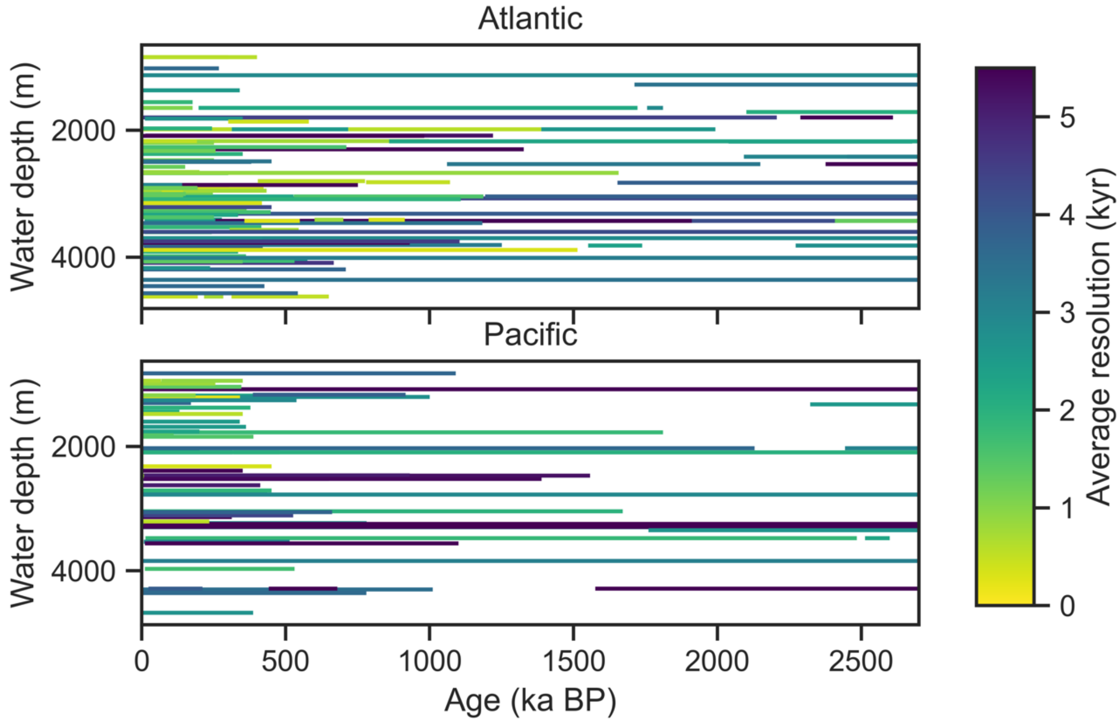

Figure S2. Overview of the BIGMACS stack input record water depth, temporal range, and average resolution, divided by ocean basins. Lighter color means the record is more densely measured (i.e., the average time spacing between samples is smaller).

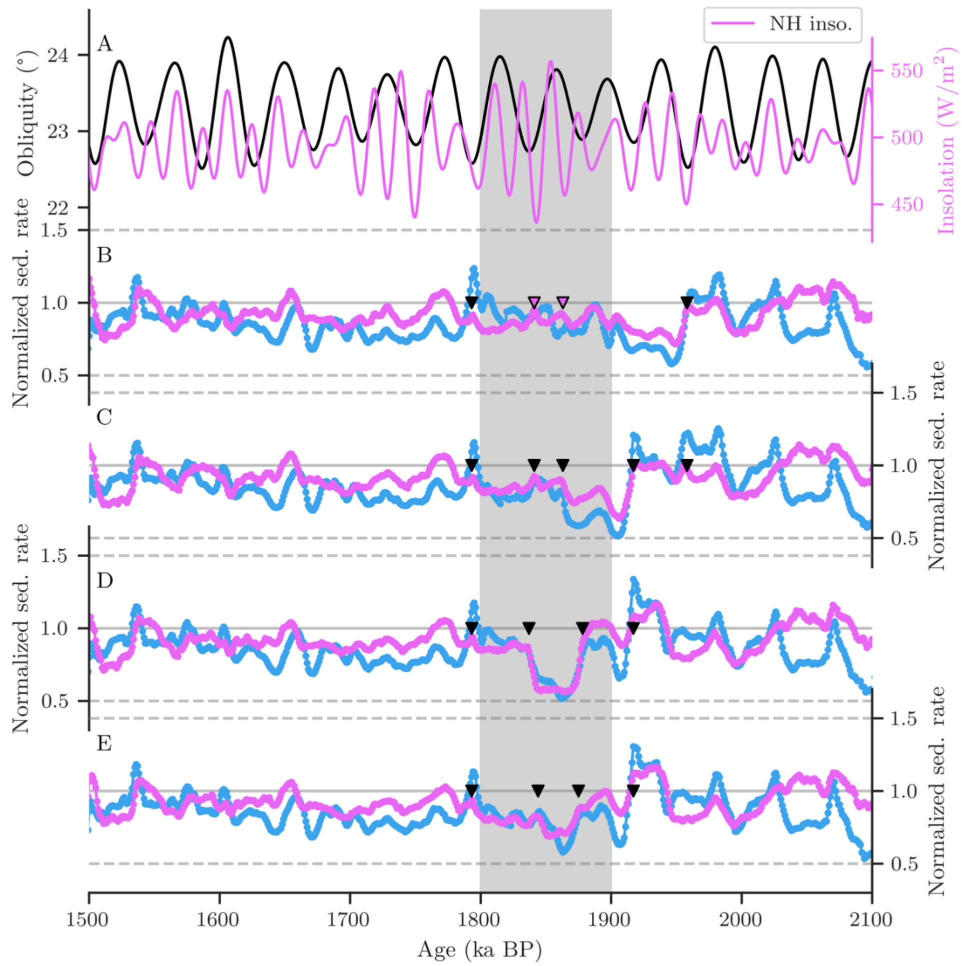

Figure S3. Basin-wide normalized sedimentation rates depending on the choices of additional age controls. (**A**) Obliquity (black line) and NH insolation (purple line) at 65° N. (**B-E**) Basin-wide normalized sedimentation rates using different additional age controls imposed on the stack construction (triangles). Purple lines are for alternate versions of the Atlantic regional stacks and blue lines are for Pacific regional stacks. Black triangles mark additional age controls imposed on both stack, and purple triangles mark additional age controls imposed only on the Atlantic stack. The main text shows the stacks constructed using the additional age controls in (B), which produce the smallest variation in normalized sedimentation rates between 1.8-1.9 Ma.

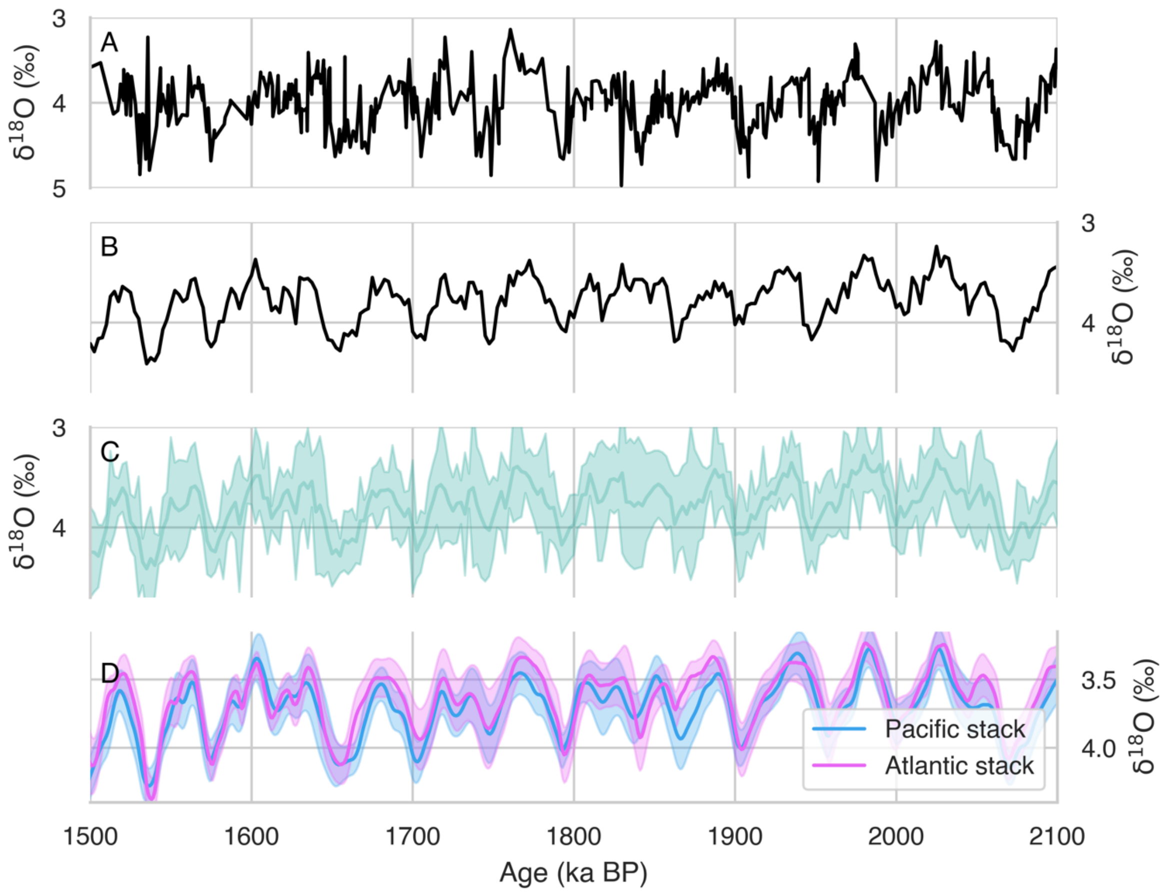

Figure S4. Stack comparison between (A) CENOGRID (Westerhold et al., 2020), (B) LR04 (Lisiecki & Raymo, 2005), (C) ProbStack (Ahn et al., 2017), and (D) the 1.5-2.1 Ma regional stacks with tie-point-guided alignments from this study.

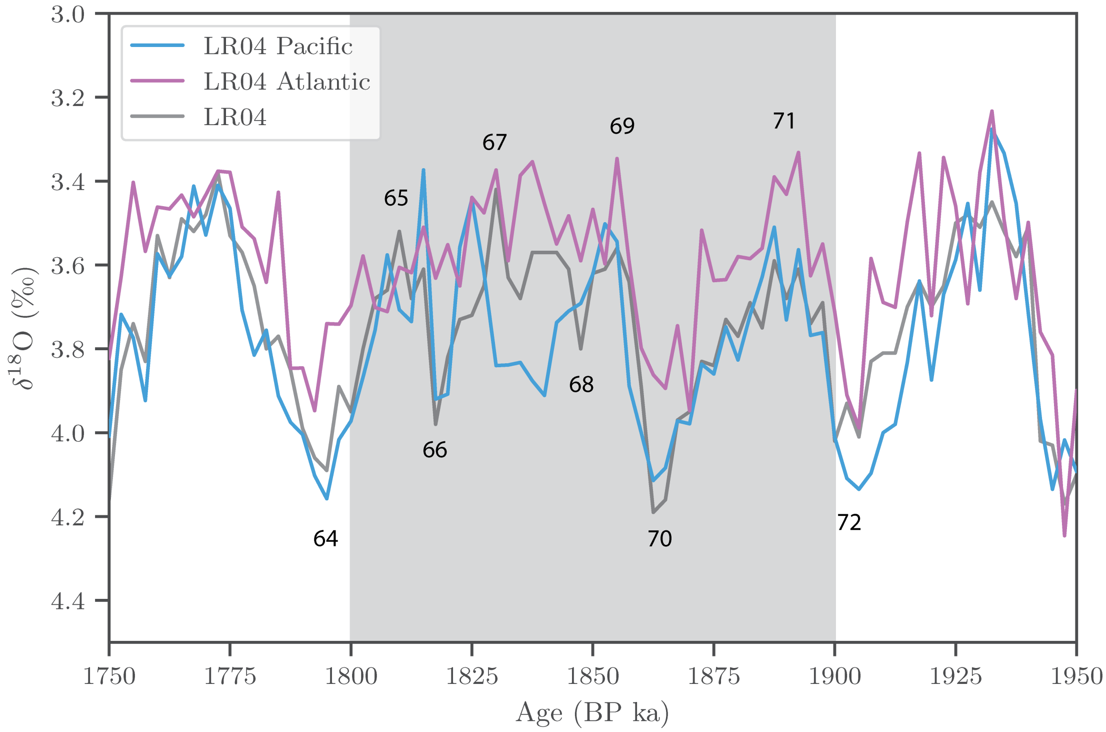

Figure S5. The LR04 global stack and separate binned stacks of its component Atlantic and Pacific records (as aligned during LR04 stack construction). The gray shade outlines the 1.8-1.9 Ma period where the Atlantic and the Pacific binned stacks diverge. Numbers denote the Marine Isotope Stages 64-72 in LR04.

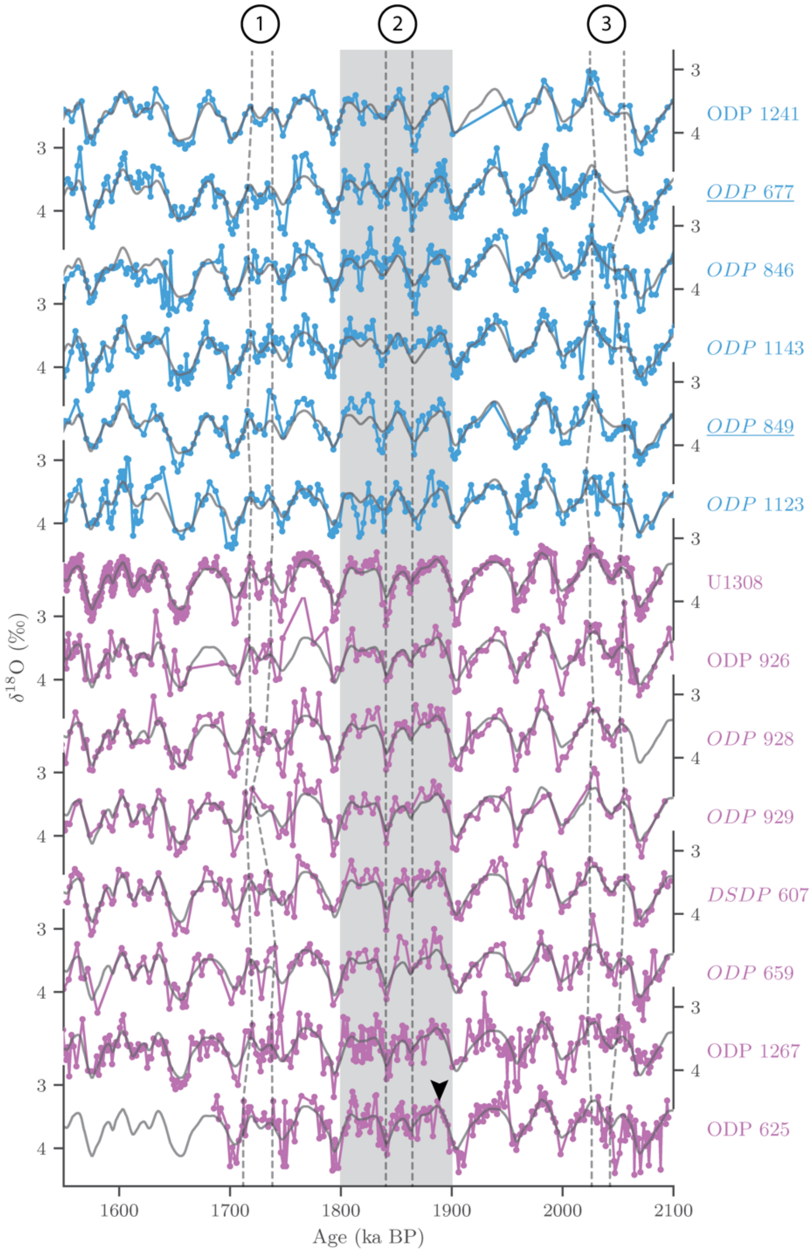

Figure S6. Visual confirmation of the BIGMACS alignment of high-resolution benthic $\delta^{18}O$ records. Records are plotted using the medians of age estimates. Blue markers are Pacific records. Purple markers are Atlantic records. Solid gray lines display the BIGMACS regional stacks (Pacific stack for the Pacific records and Atlantic stack for the Atlantic records). Feature 1 and the dashed lines below it mark the double interglacial feature. Feature 3 and the dashed lines below it mark the step interglacial feature. Feature 2 mark the pattern in the Atlantic cores, where a moderate glacial was followed by a second, relatively intense glacial. The gray shade outlines the 1.8-1.9 Ma period where the Atlantic and the Pacific records diverge. The black arrow denotes a meltwater event discovered in ODP 625 (Shakun et al., 2016). The cores with names underlined are the targets used by LR04 for alignment. The cores with names in italic are the records that were used as input for LR04.

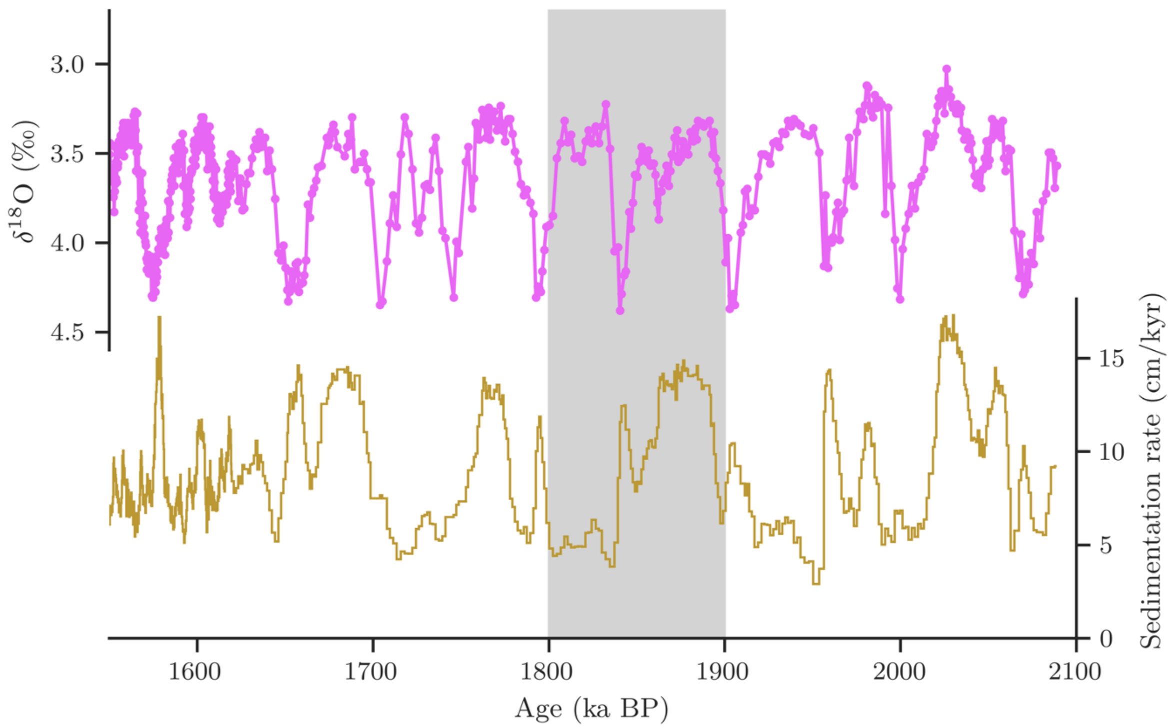

Figure S7. U1308 benthic $\delta^{18}O$ and sedimentation rate. Top: U1308 benthic $\delta^{18}O$. Bottom: U1308 sedimentation rate calculated using the BIGMACS alignment age. The gray shade outlines the 1.8-1.9 Ma period where the Atlantic and the Pacific records diverge.

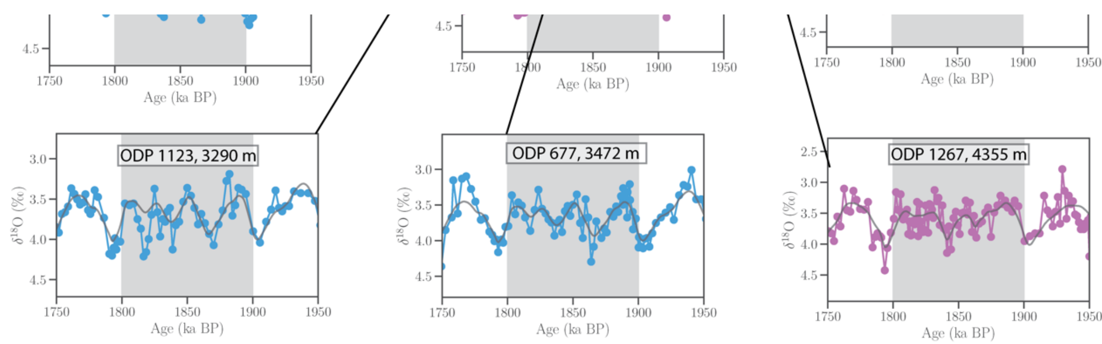

Figure S8. Same records as in Fig. S3 but shown with the locations of the cores.

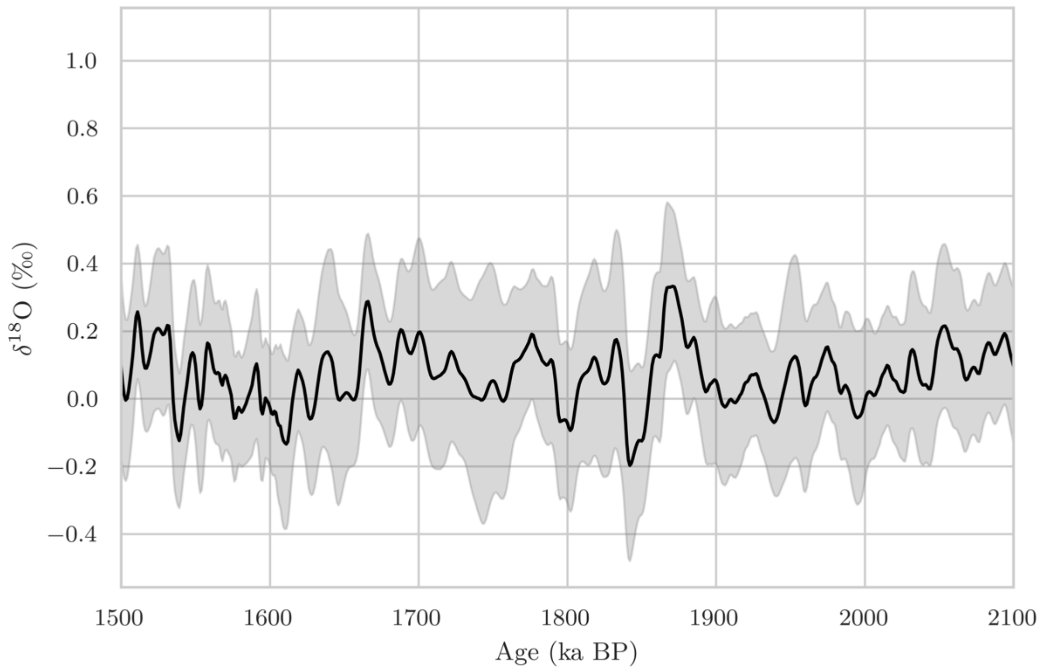

Figure S9. Time series difference between the Pacific and Atlantic stacks as shown in Fig. 2B (Pacific-Atlantic).

U1313	41	-32.9573	3426	Naafs et al. (2020)	https://doi.org/10.1029/2020PA003905
DSDP610	53.2215	-18.8868	2417	Naafs et al. (2020)	https://doi.org/10.1029/2020PA003905
AP_comp	-41.43	24.26	2669	Starr et al. (2021)	https://doi.org/10.1038/s41586-020-03094-7
U1308	49.88	-24.24	3883	Hodell and Channell (2016)	https://doi.org/10.5194/cp-12-1805-2016
U1476	-15.8	41.8	2166	Barker et al. (2022)	https://doi.org/10.1126/science.abm4033
ODP1264	-28.5327	2.8455	2507	Bell et al. (2014)	https://doi.org/10.1002/2014GC005297
ODP1267	-28.098	1.711	4355.1	Bell et al. (2014)	https://doi.org/10.1002/2014GC005297

DSDP593	-40.5086667	167.674667	1080	McClymont et al. (2016)	https://doi.org/10.1002/2016PA002954
U1483	-13.0873	121.8042	1733	Zhang et al. (2020)	https://doi.org/10.1029/2019JD032125
U1483	-13.0873	121.8042	1733	Gong et al. (2023)	https://doi.org/10.1038/s41467-023-37639-x
ODP1125	-42.55	-178.17	1365	Caballero-Gill et al. (2019)	https://doi.org/10.1029/2018PA003496
DSDP594	-45.52	174.95	1204	Caballero-Gill et al. (2019)	https://doi.org/10.1029/2018PA003496
ODP1242	7.86	-83.61	1363.4	Diz et al. (2019)	https://doi.org/10.1594/PANGAEA.909154
U1313	41	-32.9573	3426	Catunda et al. (2021)	https://doi.org/10.1594/PANGAEA.932281
U1342	54.83	176.92	818	Knudson and Ravelo (2015)	https://doi.org/10.1002/2015PA002840
MD01-2444 and U1385 combined	37.6	-10.1	2621.5	Hodell et al. (2023)	https://doi.org/10.1594/PANGAEA.951396
U1389	36.4	-7.3	644	Kaboth et al. (2017)	https://doi.org/10.5194/cp-13-1023-2017
U1387	36.8	-7.7	558	Voelker et al. (2022)	https://doi.org/10.3390/atmos13091378
U1467	4.85	73.3	487	Stainbank et al. (2020)	https://doi.org/10.1016/j.epsl.2020.116390
U1479	-35.1	17.4	2626.9	Zhao et al. (2020)	https://doi.org/10.1016/j.quascirev.2020.106643
U1446	19.084	85.735	1430	Clemens et al. (2021)	https://doi.org/10.1126/sciadv.abg3848
ODP849	0.1823	-110.519717	3839	Jakob et al. (2021)	https://doi.org/10.1029/2020PA003965
U1313	41	-32.9573	3426	Jakob et al. (2020)	https://doi.org/10.1073/pnas.2004209117
ODP981	55.4771833	-14.6508333	2173	Draut et al. (2003)	https://doi.org/10.1029/2003PA000889
ODP625	28.83	-87.16	889	Shakun et al. (2016)	https://doi.org/10.1002/2016PA002956

Table S1. Locations and references of records added to the collection by this study.

References

Ahn, S., Khider, D., Lisiecki, L. E., & Lawrence, C. E. (2017). A probabilistic Pliocene–Pleistocene stack of benthic δ^{18}O using a profile hidden Markov model. *Dynamics and Statistics of the Climate System*, *2*(1). https://doi.org/10.1093/climsys/dzx002

Barker, S., Starr, A., van der Lubbe, J., Doughty, A., Knorr, G., Conn, S., et al. (2022). Persistent influence of precession on northern ice sheet variability since the early Pleistocene. *Science*, *376*(6596), 961–967. https://doi.org/10.1126/science.abm4033

Bell, D. B., Jung, S. J. A., Kroon, D., Lourens, L. J., & Hodell, D. A. (2014). Local and regional trends in Plio-Pleistocene δ^{18}O records from benthic foraminifera. *Geochemistry, Geophysics, Geosystems*, *15*(8), 3304–3321. https://doi.org/10.1002/2014GC005297

Caballero-Gill, R. P., Herbert, T. D., & Dowsett, H. J. (2019). 100-kyr Paced Climate Change in the Pliocene Warm Period, Southwest Pacific. *Paleoceanography and Paleoclimatology*, *34*(4), 524–545. https://doi.org/10.1029/2018PA003496

Catunda, M. C. A. (2021). Oxygen isotope ratios measured on benthic foraminifera of IODP Site 306-U1313 (MIS 14-36) [Text/tab-separated-values]. PANGAEA. https://doi.org/10.1594/PANGAEA.932281

Choudhury, D., Timmermann, A., Schloesser, F., Heinemann, M., & Pollard, D. (2020). Simulating Marine Isotope Stage 7 with a coupled climate–ice sheet model. *Climate of the Past*, *16*(6), 2183–2201. https://doi.org/10.5194/cp-16-2183-2020

Clemens, S. C., Yamamoto, M., Thirumalai, K., Giosan, L., Richey, J. N., Nilsson-Kerr, K., et al. (2021). Remote and local drivers of Pleistocene South Asian summer monsoon precipitation: A test for future predictions. *Science Advances*, *7*(23), eabg3848. https://doi.org/10.1126/sciadv.abg3848

Diz, P., Peñalver-Clavel, I., Hernández-Almeida, I., & Bernasconi, S. M. (2019). Oxygen isotopes of benthic foraminifera of ODP Site 202-1242 [Text/tab-separated-values]. PANGAEA. https://doi.org/10.1594/PANGAEA.909154

Draut, A. E., Raymo, M. E., McManus, J. F., & Oppo, D. W. (2003). Climate stability during the Pliocene warm period. *Paleoceanography*, *18*(4). https://doi.org/10.1029/2003PA000889

Gong, L., Holbourn, A., Kuhnt, W., Opdyke, B., Zhang, Y., Ravelo, A. C., et al. (2023). Middle Pleistocene re-organization of Australian Monsoon. *Nature Communications*, *14*(1), 2002. https://doi.org/10.1038/s41467-023-37639-x

Hodell, D. A., & Channell, J. E. T. (2016). Mode transitions in Northern Hemisphere glaciation: co-evolution of millennial and orbital variability in Quaternary climate. *Climate of the Past*, *12*(9), 1805–1828. https://doi.org/10.5194/cp-12-1805-2016

Hodell, D. A., Crowhurst, S. J., Lourens, L., Margari, V., Nicolson, J., Rolfe, J. E., et al. (2023). A 1.5-million-year record of orbital and millennial climate variability in the North Atlantic. *Climate of the Past*, *19*(3), 607–636. https://doi.org/10.5194/cp-19-607-2023

Jakob, K. A., Wilson, P. A., Pross, J., Ezard, T. H. G., Fiebig, J., Repschläger, J., & Friedrich, O. (2020). A new sea-level record for the Neogene/Quaternary boundary reveals transition to a more stable East Antarctic Ice Sheet. *Proceedings of the National Academy of Sciences*, *117*(49), 30980–30987. https://doi.org/10.1073/pnas.2004209117

Jakob, K. A., Ho, S. L., Meckler, A. N., Pross, J., Fiebig, J., Keppler, F., & Friedrich, O. (2021). Stable Biological Production in the Eastern Equatorial Pacific Across the Plio-Pleistocene Transition (~3.35–2.0 Ma). *Paleoceanography and Paleoclimatology*, *36*(4), e2020PA003965. https://doi.org/10.1029/2020PA003965

Kaboth, S., Grunert, P., & Lourens, L. (2017). Mediterranean Outflow Water variability during the Early Pleistocene. *Climate of the Past*, *13*(8), 1023–1035. https://doi.org/10.5194/cp-13-1023-2017

Knudson, K. P., & Ravelo, A. C. (2015). North Pacific Intermediate Water circulation enhanced by the closure of the Bering Strait. *Paleoceanography*, *30*(10), 1287–1304. https://doi.org/10.1002/2015PA002840

Lee, T., Rand, D., Lisiecki, L. E., Gebbie, G., & Lawrence, C. (2023). Bayesian age models and stacks: combining age inferences from radiocarbon and benthic δ^{18}O stratigraphic alignment. *Climate of the Past*, *19*(10), 1993–2012. https://doi.org/10.5194/cp-19-1993-2023

Lisiecki, L. E., & Raymo, M. E. (2005). A Pliocene-Pleistocene stack of 57 globally distributed benthic δ^{18}O records. *Paleoceanography*, *20*(1), 1–17. https://doi.org/10.1029/2004PA001071

Lisiecki, L. E., & Stern, J. V. (2016). Regional and global benthic δ18O stacks for the last glacial cycle. *Paleoceanography*, *31*(10), 1368–1394. https://doi.org/10.1002/2016PA003002

McClymont, E. L., Elmore, A. C., Kender, S., Leng, M. J., Greaves, M., & Elderfield, H. (2016). Pliocene-Pleistocene evolution of sea surface and intermediate water temperatures from the southwest Pacific. *Paleoceanography*, *31*(6), 895–913. https://doi.org/10.1002/2016PA002954

Naafs, B. D. A., Voelker, A. H. L., Karas, C., Andersen, N., & Sierro, F. J. (2020). Repeated Near-Collapse of the Pliocene Sea Surface Temperature Gradient in the North Atlantic. *Paleoceanography and Paleoclimatology*, *35*(5), e2020PA003905. https://doi.org/10.1029/2020PA003905

Renaudie, J., Lazarus, D. B., & Diver, P. (2020). NSB (Neptune Sandbox Berlin): An expanded and improved database of marine planktonic microfossil data and deep-sea stratigraphy. *Palaeontologia Electronica*, *23*(1), 1–28. https://doi.org/10.26879/1032

Shakun, J. D., Raymo, M. E., & Lea, D. W. (2016). An early Pleistocene Mg/Ca-δ18O record from the Gulf of Mexico: Evaluating ice sheet size and pacing in the 41-kyr world. *Paleoceanography*, *31*(7), 1011–1027. https://doi.org/10.1002/2016PA002956

Stainbank, S., Spezzaferri, S., De Boever, E., Bouvier, A.-S., Chilcott, C., De Leau, E. S., et al. (2020). Assessing the impact of diagenesis on foraminiferal geochemistry from a low latitude, shallow-water drift deposit. *Earth and Planetary Science Letters*, *545*, 116390. https://doi.org/10.1016/j.epsl.2020.116390

Starr, A., Hall, I. R., Barker, S., Rackow, T., Zhang, X., Hemming, S. R., et al. (2021). Antarctic icebergs reorganize ocean circulation during Pleistocene glacials. *Nature*, *589*(7841), 236–241. https://doi.org/10.1038/s41586-020-03094-7

Voelker, A. H. L., Rodrigues, T., Trotta, S., Marino, M., & Kuhnert, H. (2022). A Southern Portuguese Margin Perspective of Marine Isotope Stage 47—An Interglacial in the 41 kyr World. *Atmosphere*, *13*(9), 1378. https://doi.org/10.3390/atmos13091378

Westerhold, T., Marwan, N., Drury, A. J., Liebrand, D., Agnini, C., Anagnostou, E., et al. (2020). An astronomically dated record of Earth's climate and its predictability over the last 66 million years. *Science*, *369*(6509), 1383–1387. https://doi.org/10.1126/science.aba6853

Zhang, P., Xu, J., Holbourn, A., Kuhnt, W., Beil, S., Li, T., et al. (2020). Indo-Pacific Hydroclimate in Response to Changes of the Intertropical Convergence Zone: Discrepancy on Precession and Obliquity Bands Over the Last 410 kyr. *Journal of*

Geophysical Research: Atmospheres, *125*(14), e2019JD032125. https://doi.org/10.1029/2019JD032125

Zhao, X., Koutsodendris, A., Caley, T., & Dupont, L. (2020). Hydroclimate change in subtropical South Africa during the mid-Piacenzian Warm Period. *Quaternary Science Reviews*, *249*, 106643. https://doi.org/10.1016/j.quascirev.2020.106643